

# Stirring, mixing, growing: microscale processes change larger scale phytoplankton dynamics.

Francesco Paparella,<sup>1\*</sup> Marcello Vichi<sup>2</sup>

<sup>1</sup>Division of Sciences and Mathematics, Center on Stability, Instability  
and Turbulence, New York University Abu Dhabi,  
Saadyat Island, Abu Dhabi, UAE

<sup>2</sup>Department of Oceanography and Marine Research Institute, University of  
Cape Town  
Cape Town, Rondebosch 7701, South Africa

\*To whom correspondence should be addressed; E-mail:  
francesco.paparella@nyu.edu.

## Abstract

The quantitative description of marine systems is constrained by a major issue of scale separation: most marine biochemical processes occur at sub-centimeter scales, while the contribution to the Earth’s biogeochemical cycles is expressed at much larger scales, up to the planetary one. In spite of vastly improved computing power and observational capabilities, the modeling approach has remained anchored to an old view that sees the microscales as unable to substantially affect larger ones. The lack of a widespread theoretical appreciation of the interactions between vastly different scales has led to the proliferation of numerical models with uncertain predictive capabilities. We show that an enhanced Lagrangian modeling framework, allowing for those interactions, can easily tackle puzzling problems such as the phenology of phytoplankton blooms, or vertical variability in mixed layers.

## Introduction

Marine phytoplankton is involved in several biogeochemical processes at the microbial ocean scale that affect entire ecosystems [1, 2]. Predictive models of phytoplanktonic processes are thus fundamental to many applications. In climate projections, the “biological pump” is a fundamental component of the carbon cycle [3, 4], described by modeling phytoplankton primary production and the net export of organic matter through the marine food web and the water column. Models of biogeochemical and phytoplankton processes are also employed in operational oceanography and coastal man-

agement [5, 6]. Predictive models of coastal and near-shore transport are coupled with water quality and biogeochemical models to provide forecasts of undesirable disturbances such as eutrophication, hypoxia, or harmful algal blooms. Ultimately, the outputs of these models are used for fishery management, end-to-end ecosystem models, and indicators of ocean health [7, 8].

There is, however, a fundamental difficulty in the modeling process: namely, the chasm between the scales where the biogeochemical processes occur and are being observed (by probes deployed in the ocean, laboratory experiments or metagenomics studies [1, 9, 2]) and the scales where the system response is sought, observed and interpreted (by remote sensing, data aggregation and models). Laboratory experiments such as cultures and mesocosms allow to empirically estimate a model’s biological terms, upon the assumption of homogeneous distribution of all the biochemical fields [10, 11], while neglecting the physical terms. The interactions between these terms is ultimately mandated to the numerical solution of coupled physical-biogeochemical models [12, 13], which cannot include all the spatial and temporal scales necessary to close the chasm.

In this paper, we address the theory behind marine physical-biogeochemical models, we expose some limits of the current models, and we propose a new approach. To make our point, we focus on the open ocean mixed layer and phytoplankton dynamics, which is at the base of the water column biogeochemistry [2].

The distribution of plankton shows variability from the global scale down to the microscale (centimetric lengths) [14, 15]. Plankton patchiness at the

mesoscale and sub-mesoscale is shaped by the interaction between biological growth processes and turbulent lateral stirring linked to upper ocean frontal eddies and currents [16, 17, 18]. Lateral stirring and mixing alone cannot generate patchiness [16]. A triggering mechanism is needed, and physics-driven processes affecting the vertical structure of the mixed layer (that is, on scales smaller than 100 m) may easily fulfill this role. This variability, in turn, is enhanced by biological processes such as the interplay between light and nutrient gradients, cell buoyancy adjustments, gyrotaxis, convergent swimming, and light-dependent grazing [19, 20, 21, 22]. The emerging very-high-resolution sampling techniques suggest that plankton remains patchy at the scales of one meter both in the vertical and in the horizontal [23], and that homogeneity might not be reached before the centimeter scales [24, 25, 23]. As we shall see, models assuming homogeneity at the fine and micro scales may easily incur in serious biases.

Three classes of processes should be included to model marine biogeochemical processes at the microscale: turbulent stirring, caused by fluid eddies, which displaces, stretches, and folds water volumes, increasing the gradients of the transported fields; irreversible mixing, caused by sub-microscale processes, which decreases these gradients; and growth (or decay) which changes the concentration of the fields by chemical or biological means. In principle, these processes must correspond to distinct terms in the equations resolved by numerical models. In practice, two broadly-defined formulation may be used to build a model: the Eulerian and the Lagrangian. Choosing the formulation binds the model equations to conform to a set of approximations which may not strictly abide to this principle.

The majority of model applications mentioned above are Eulerian [10, 26, 27, 28]. In this formulation, all three processes occur at the nodes of a fixed spatial grid, where all the relevant fields are located (Fig. 1A). Invoking the continuum approximation, the biological variables are approximated as smoothly varying mean fields whose values at the grid nodes are representative of the average values in the grid cell [27]. An important feature of Eulerian models is that the unresolved turbulent stirring processes are assimilated to irreversible mixing. While this practice may achieve satisfactory results for non-reacting, passively transported tracers, it yields questionable, if not flawed, results for biological and chemical tracers, because it hopes that the biological response to the simulated Eulerian mean field is the same as the average response to the real, unresolved, patchy environment [29, 30].

Other models use the Lagrangian formulation, which singles-out either small portions of the fluid or individual biological agents, and follows them along their motion (Fig. 1B). Despite their approximations (e.g. number of particles insufficient to resolve all the fluid structures and use of stochastic processes to mimic turbulence), Lagrangian models describe stirring processes as such, rather than assimilating their effect to irreversible mixing. In plankton modeling, the Lagrangian formulation, originally identified with the term Lagrangian ensemble [31, 32, 33, 34], is often referred to as individual based modeling [35]. We argue that a clear distinction should be made between single cell Lagrangian models [36, 37], in which the movement of a single individual is followed, but growth/death processes and cell division are not included, and Lagrangian ensembles (Fig. 1B), where the super-individual concept [38] is used to describe the plankton population dynam-

ics. Some authors have stated the superiority of the Lagrangian approach in describing plankton dynamics [34, 39, 40, 30].

However, there are intrinsic limitations to applying the super-individual concept to the modeling of phytoplankton communities, because a Lagrangian ensemble is not conceived to exchange with surrounding ensembles any of the active agents that it carries (Fig. 1B). Therefore, nearly all Lagrangian models (but see [41]) neglect to include irreversible mixing processes. In the sporadic cases where Lagrangian and Eulerian formulations have been compared, this issue appears to have been overlooked [32, 42, 43, 44, 30], even though it may lead to unrealistic, even paradoxical outcomes.

Consider a region of ocean with steady conditions, favorable for a phytoplankton bloom. Assume an initial random distribution dividing the fluid in very small patches, half devoid of phytoplankton, and the others at carrying capacity. The ensembles of a Lagrangian model would mimic these patches, but, lacking any mutual interaction, plankton in those already at carrying capacity would never reach the nearby empty ones and trigger growth. The ensembles lacking phytoplankton would remain devoid of it, and the others would stay at the carrying capacity. The bulk concentration, computed as an average over all the Lagrangian ensembles, would indefinitely remain at one half of the carrying capacity: a baffling outcome given the favorable conditions! In an Eulerian model, irreversible mixing would quickly offset from zero the concentration of the empty nodes, triggering growth, so that the bulk concentration will eventually reach the carrying capacity. However, if the initial subdivision of empty and full patches were too fine to be resolved, then

the amount of irreversible mixing computed by the Eulerian model would be a gross overestimation of the real one, which begs the question whether the modeled growth rate of the bulk concentration is realistic [30].

Turbulent stirring, irreversible mixing, and growth are each associated to their own distinct time scales. For example, the celebrated Sverdrup model [45] for the onset of phytoplanktonic blooms stems from the assumption that the growth time scale is slower than the stirring time scale. It is of extreme historical importance, and is the founding stone that all later bloom models have confronted, either to build on it, or to overthrow it [46, 47]. It also has a peculiar feature: owing to its linearity, substituting stirring with irreversible mixing (if characterized by the same time scales as the stirring) leaves the results unchanged. As we shall illustrate in the following, in the presence of nonlinear biological terms, this equivalence is lost: in Sverdrup-like nonlinear models, the separation between the time scales of stirring and of irreversible mixing determines the tempo and mode of the bulk phytoplankton growth. The proliferation of explanations for the occurrence of blooms, often distinct from each other by subtle details, may be a symptom of the lack of appreciation for a key theoretical issue: phytoplankton patchiness affects the bulk growth.

Occasionally, some attempts have been made to parameterize patchiness effects into Eulerian biogeochemical models. Realizing that the biological response is greatly affected by the treatment of the unresolved scales, authors like Fennel [48] have long proposed to use “effective” biological parameters. A time-delay parameterization was suggested for the case where patchiness is the result of an oscillatory population dynamics occurring with different

phases in different places [49]. More recently, a closure parameterization was introduced, reminiscent of those used for turbulence [50]. The approach is formally valid only when the fluctuations are small, which high resolution chlorophyll profiles suggest is not the case [51]. Overall, the bulk of the literature appears to overlook the issue, treating biogeochemical tracers in the same way as non reacting ones.

We argue that the strategy of replacing unresolved transport with irreversible mixing, and then compensate the resulting biases by means of some parameterization, will face overwhelming difficulties. For example because different initial conditions, keeping everything else the same, may yield different bulk growth rates [29] (an issue also noted in the early work on the plankton patchiness theory [16]).

If turbulent stirring, irreversible mixing, and growth processes are modeled separately and independently from each other, then reproducing realistic phytoplankton dynamics in predictive models should become much easier. A class of Lagrangian methods recently proposed [29] achieves this goal by depicting Lagrangian particles as representing microscale-sized, homogeneous control volumes of water, rather than individual organisms or ensembles. In this framework, irreversible mixing processes are represented by exchanging small mass fluxes between nearby particles. We call *aquacosms* such Lagrangian particles subject to coupling fluxes (Fig. 1C, see “methods” for details). The coupling is regulated by a parameter,  $p$ , whose value is proportional to the intensity of the fluxes. As we shall demonstrate,  $p$  sets the time scale associated with the irreversible destruction of biogeochemical variance at the microscales, which, in this approach, remains independent of the time



scales of mechanical stirring. Results analogous to those of Lagrangian ensemble models are recovered for uncoupled particles ( $p = 0$ ). In the opposite limit, high values of  $p$  produce an excessive irreversible mixing, and yield results strongly resembling Eulerian simulations.

## Results

In the following we examine the results obtained with water-column models, considering first a few idealized cases, and then more realistic open ocean situations from the North Pacific and the Southern Ocean. We compare an Eulerian model, where vertical turbulent stirring is parameterized by eddy diffusivity, with Lagrangian aquacosm models, distinguished by different intensities of the microscale irreversible mixing, where vertical turbulent stirring is modeled as stochastic motions of the aquacosms, matching the Eulerian eddy diffusivity.

### Pure stirring and mixing

First, we shall consider the case of turbulent stirring and mixing of a substance not subject to any reaction. In non-dimensional units, the eddy-diffusive Eulerian model is

$$\frac{\partial C}{\partial t} = \frac{\partial^2 C}{\partial z^2} \quad (1)$$

with  $C$  representing the concentration of the non-reactive substance, subject to no-flux boundary conditions in the water column  $0 < z < 1$ . In this formulation, turbulent stirring is completely replaced by irreversible mixing,

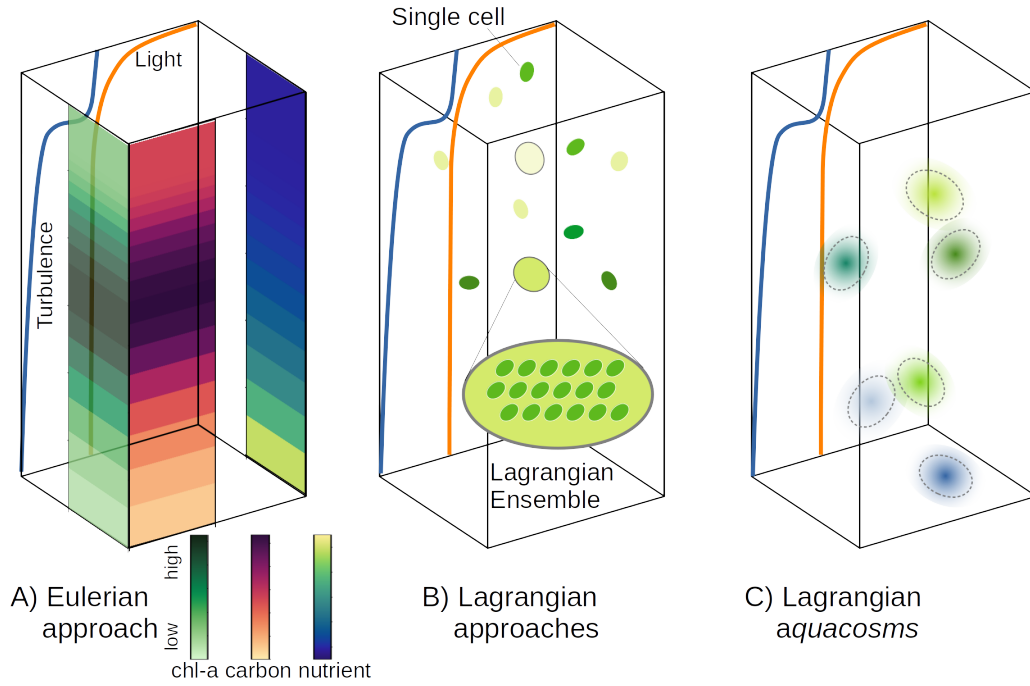


Figure 1: Schematic of different phytoplankton modeling approaches. **A)** The vertical distribution of phytoplankton carbon and chlorophyll can be simulated according to vertical nutrient and light gradients and a turbulent field. The Eulerian approach samples all active fields at the nodes of a fixed grid; fine and microscale stirring (turbulence) is modeled as irreversible mixing, wiping out fine and microscale patchiness. **B)** The Lagrangian Ensemble approach bundles individual cells into Lagrangian particles; the number of organisms per particle is modified by infra-particle ecological interactions; unresolved turbulence is modeled as a stochastic motion of the particles, which don't interact with each other. **C)** The Lagrangian aquacosm approach tracks tiny Lagrangian water masses (*aquacosms*) moving as in B); biogeochemical interactions occur within aquacosms, which are permeable, thus allowing for mass exchanges between nearby aquacosms.

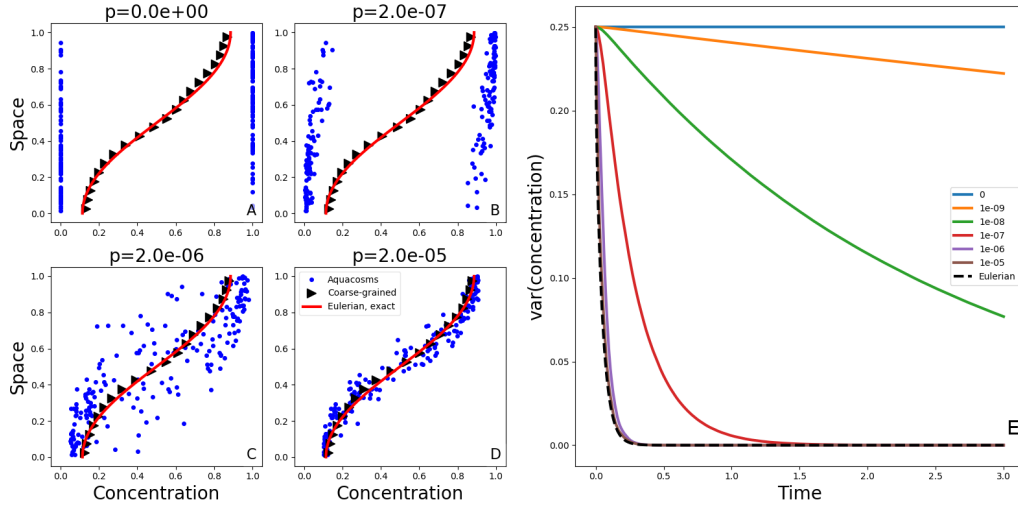


Figure 2: **A-D)** Exact solutions at time  $t = 0.05$  of the diffusion equation (1) with the initial condition (2) and no-flux boundary conditions (red lines). The blue dots show the position and the concentration of the Lagrangian particles for equivalent aquacosm simulations with the same diffusivity and varying coupling strength  $p$ . The black triangles are a coarse-grained version of the same data, obtained with a Gaussian kernel estimator with standard deviation 0.1 (see methods). **E)** variance, as a function of time, in Lagrangian aquacosm simulations with varying coupling strength  $p$  (solid lines) and variance of the exact solution of the Eulerian problem (1) (dashed line).

described mathematically by the right-hand side term of the equation. As the initial condition, we choose the step function

$$C(z, 0) = \begin{cases} 0, & z < 1/2 \\ 1, & z \geq 1/2 \end{cases}. \quad (2)$$

In the Lagrangian aquacosm approach, just as in other Lagrangian methods, turbulent stirring is modeled as a Brownian motion which scrambles the position of the particles. Irreversible mixing is modeled separately and its intensity is determined by the value of the coupling parameter  $p$  (see methods). The aquacosms (Lagrangian particles) are initially placed at uniformly random position within the domain, those in the first half take a concentration of zero, the others take a concentration of one.

Figures 2A-D show the concentration and position of the aquacosms for different values of the coupling parameter  $p$ , together with the analytical solution of equation (1). Brownian motion produces patchiness: a random alternation of particles with high and low concentration values. Irreversible mixing equalizes the concentration of nearby particles, thus removing patchiness, more and more effectively as the coupling strength  $p$  increases. Local weighted averages of the Lagrangian result (black triangles, see methods), are essentially identical to the analytic solution of the Eulerian model. This coincidence might suggest that the Eulerian and all of the Lagrangian models are equivalent. The coarse-graining process of taking local averages, however, gives only a partial picture. Panels A-D do not depict equivalent microphysics. The concentration carried by the individual particles (which,

ultimately, is all that matters for the reaction terms when they are present) is vastly different in the four cases. The amount of irreversible mixing, set by the parameter  $p$ , determines how quickly the fluctuations around the local averages are dissipated (Fig. 2E), that is,  $p$  sets the time scale associated to irreversible mixing processes. When irreversible mixing is strong (high values of  $p$ ) the fluctuations around the local means, thus variance, decay just as quickly as in the Eulerian case. For smaller values of  $p$  the time scale of variance decay can be made arbitrarily large: fluctuations may persist even when the local averages suggest the presence of a vertically near-uniform profile of concentration. In the limit case  $p = 0$  (uncoupled particles) each aquacosc maintains its initial concentration, and variance remains constant in time, even though the local averages still tend to uniformity, as prescribed by (1).

## Sverdrup's model expanded

Next we add to equation (1) a simple logistic growth term. In dimensional units our model is

$$\frac{\partial C}{\partial t} = \kappa \frac{\partial^2 C}{\partial z^2} + r f(z) C \left(1 - \frac{C}{K}\right) \quad (3)$$

where  $\kappa$  is the eddy diffusivity, assumed to be constant, and  $r$  is the maximum growth rate of phytoplankton, having concentration  $C$  and carrying capacity  $K$ . Zero-flux boundary conditions are imposed at both ends of the water column, that is at  $z = 0$  and  $z = \ell$ . This model is more general than Sverdrup's original one, as it does not yet make any assumption on the relative size of the turbulent stirring and biological time scales, and it includes

a nonlinear growth/loss term. However, it still parameterizes stirring with an eddy diffusion term, thus interchanging stirring with irreversible mixing. The non-dimensional function  $f$  quantifies the balance between light-stimulated growth, and loss of biomass due to respiration. Sverdrup defined it as

$$f(z) = e^{-\lambda z} - \frac{\mu}{r}, \quad (4)$$

where  $\mu$  is a constant respiration rate, and  $\lambda$  is a measure of water transparency, but Sverdrup's argument holds for any integrable function  $f$  sandwiched between  $O(1)$  bounds. Choosing  $\ell$  as the unit of length,  $\ell^2/\kappa$  as the unit of time, and  $K$  as the unit of concentration, equation (3) takes the non-dimensional form:

$$\frac{\partial C}{\partial t} = \varepsilon f(z)C(1 - C) + \frac{\partial^2 C}{\partial z^2}. \quad (5)$$

The parameter  $\varepsilon = r\ell^2/\kappa$  expresses the ratio of the stirring/mixing and the biological time scales (the former quantified through the eddy diffusivity as  $\ell^2/\kappa$ ). Formally, Sverdrup's approximation applies for vanishing  $\varepsilon$ , when one can argue that physics and biology disentangle: in that case, the eddy diffusion term makes the initial condition vertically homogeneous after a transient no longer than  $O(1)$ , keeping the concentration  $C$  independent of depth at all later times. Then, on  $O(\varepsilon^{-1})$  time scales, the vertically constant concentration changes in time according to the ODE

$$\dot{C} = \varepsilon I C(1 - C) \quad (6)$$

where  $I$  is the integral of  $f$  over the water column and the dot denotes a derivative with respect to time. In practice, this argument yields a good approximation up to  $\varepsilon \approx 1$ .

In our Lagrangian formulation of this problem the aquacosms move by performing a Brownian motion. The concentration in each aquacosm is determined by the ODE associated with the reaction term in (5), and by the coupling fluxes modeling irreversible mixing (see methods). If the growth term is linearized, then the eddy-diffusive Eulerian and the Lagrangian approach are equivalent in a coarse-grained sense (as partly observed by other authors [42, 43]), but we show here, and demonstrate analytically in sec. S1 of the supplementary materials, that nonlinear biological terms break down the equivalence.

Figure 3 shows the phytoplankton concentration mean and variance as a function of time for equation (5) and its aquacosm counterpart, with  $f(z) = 1$ , the initial condition (2), and two values of the ratio  $\varepsilon = 0.1$  and  $\varepsilon = 1$ . As sketched in the introduction, because all fluid parcels are initially set at a fixed point of the reaction terms, with uncoupled particles ( $p = 0$ , as in a Lagrangian ensemble model) the mean unrealistically remains at one half of the carrying capacity despite the positive growth rate. When the coupling between the aquacosms is switched on, the mean gradually tends to the carrying capacity ( $C = 1$ ) and the variance tends to zero. The rapidity with which the asymptotic values are approached depends on the strength of the coupling parameter  $p$ : high values produce results that behave just as predicted by Sverdrup's theory, but small ones produce growth curves that are nothing like the solution of the ODE associated with the reaction

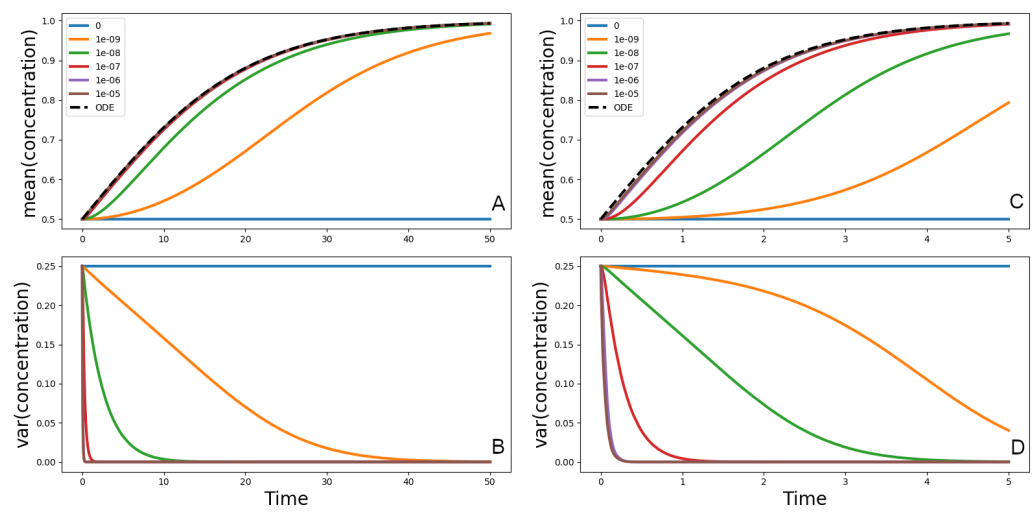


Figure 3: **(A, C)** Average plankton concentration and **(B, D)** variance, as a function of time, for the problem (5) with  $f(z) = 1$ ,  $\varepsilon = 0.1$  (A, B) or  $\varepsilon = 1$  (C, D) and the step initial condition (2). The solid lines refer to Lagrangian aquacosc simulations with varying strength of the coupling parameter  $p$ . The dashed line is the solution of Sverdrup's approximation (6). Note the different ranges of the time axes.

term. Because Sverdrup's theory postulates the equivalence of stirring and irreversible mixing, the time scales of the two kind of processes are the same: a water parcel devoid of plankton and one full of plankton equalize their concentration within the stirring time scale. When stirring and mixing are treated as separate processes, with the second allowed to be slower than the first, parcels lacking plankton are constantly seeded by the full ones, and the overall rate of growth is determined by a delicate interplay of biological processes, turbulent stirring and irreversible mixing. Lagrangian ensemble models only account for the first, and eddy-diffusive Eulerian models are dominated by the second. We notice that in a generic non-homogeneous environment with concurrent stirring, mixing and growing, there is no reason to expect that the bulk phytoplankton concentration is described solely by



the ODE associated with the reaction terms.

The examples so far show that the fast stirring of a step-like initial condition produces patchiness, which then affects the bulk growth rate. Much attention has been given to the case of non-homogeneous biological growth (e.g. using the form (4) for  $f(z)$ ) when growth is faster than stirring. Then, according to the critical turbulence theory [52, 53, 54], phytoplankton closer to the surface contributes to the overall growth more than Sverdrup's theory would provide for, so that a bloom may initiate even when the average light would not allow for that. Differences in light history and acclimation have also been affirmed to produce growth when Sverdrup's theory would predict decay [42, 33, 55]. What has not been stressed is that these conditions would also naturally lead to the creation of patchiness if irreversible mixing processes are not fast enough to remove it. When growth is faster than turbulent stirring, then the phytoplankton in water parcels at shallow depth will have time to grow substantially more than that in the deeper parcels spending some time in darkness. As stirring makes some of the shallow particles sink and replaces them with some of those that were at depth, then microscale patchiness ensues. Just as in the case of a step-like initial condition, patchiness affects growth. As the bloom progresses, water parcels having spent the most time close to the surface reach the carrying capacity before the others, and the rapidity of the bulk growth becomes regulated by the intensity of the irreversible mixing, which transfers plankton from high to low concentration particles.

This process is illustrated in Fig. 4 for different degrees of the coupling between aquacosms. In the linear regime, when phytoplankton concentration

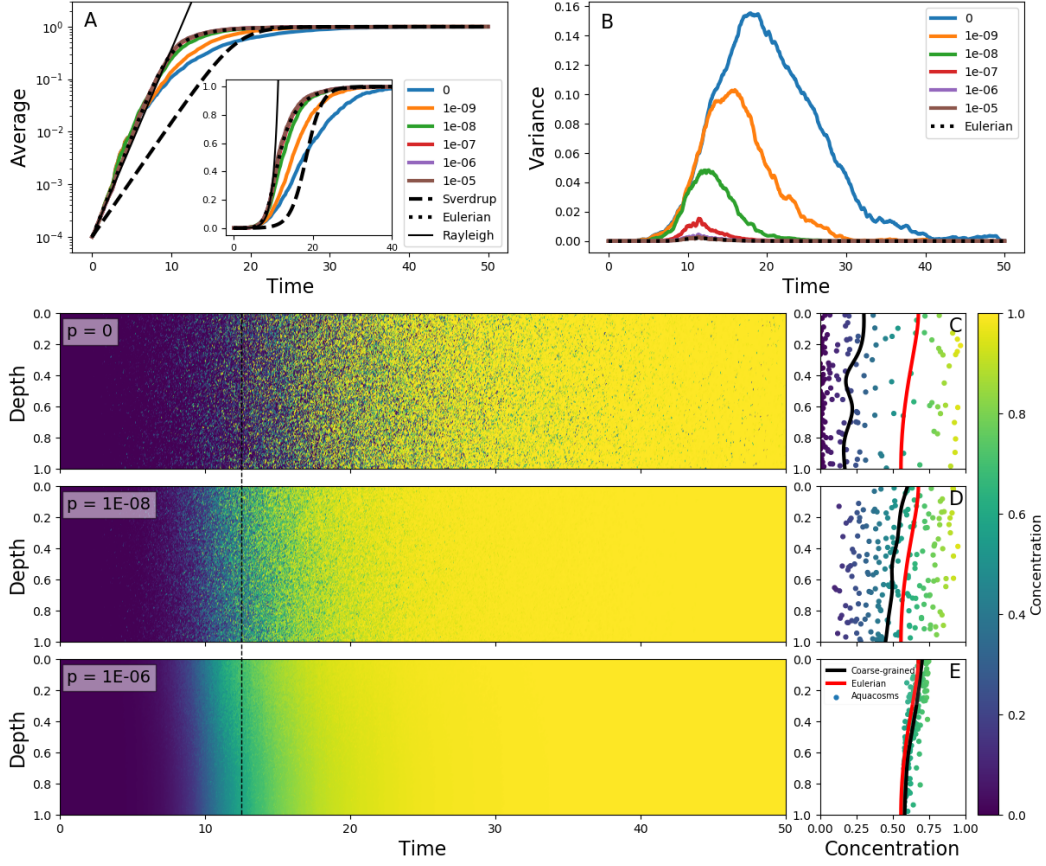


Figure 4: **(A)** Average phytoplankton concentration and **(B)** variance as a function of time, for the Eulerian problem (5) with  $f(z) = e^{-z/0.15} - 0.1$ ,  $\varepsilon = 10$  and constant-in-space initial condition  $C(z) = 10^{-4}$  (dotted lines). The solid lines in color refer to Lagrangian aquacosm simulations with the same parameters, with varying coupling strength  $p$ . The dashed line is the solution of Sverdrup’s approximation (6). The thin black line is an exponential growth with a rate estimated by means of the Rayleigh quotient (sec.S2 in supp. mat.) associated to equation (5). The inset shows the same data as panel A, but with a linear, rather than logarithmic, vertical axis. **(Lower panels)** plankton concentration as a function of depth and time for Lagrangian simulations with  $p = 0, 10^{-8}, 10^{-6}$ . **(C-E)** concentration and depth of the aquacosms (dots), coarse-grained concentration of the aquacosms (black line) and numerical solution of the Eulerian model (red line) at the time marked by the dashed black line in the left panels.

is much smaller than the carrying capacity, the Eulerian model (5) and all the Lagrangian models show the same growth rate of the bulk concentration (Fig. 4A), which is in excess of what Sverdrup’s theory would dictate. This is in agreement with the critical turbulence prescriptions (see sec. S2 of supplementary materials) as long as the process is linear. In the nonlinear regime, the Lagrangian models yield distinct results: with small coupling strength, variance grows with time (Fig. 4B), and this leads to bulk growth significantly slower than in the eddy-diffusive Eulerian model, due to the patchy environment. Once again, destroying the variance by using a strong enough coupling parameter recovers the results of the Eulerian model. Figure 4C-E shows that variance genuinely corresponds to patchiness: with low  $p$ , aquacosms of starkly different concentration are found next to each other, and the coarse-grained equivalence of Lagrangian and Eulerian models is lost.

## Microscales and phytoplankton phenology

To demonstrate the effect of irreversible mixing on phytoplankton phenology, we run an eddy-diffusive Eulerian model and Lagrangian aquacosm models. They use realistic eddy diffusivity profiles and incident solar radiation data spanning one year, representative of the conditions found at Ocean Station PAPA in the north-east Pacific Ocean and in the sub-Antarctic zone of the Southern Ocean, and a simplified version of a biogeochemical model currently used in ocean climate simulations, where light availability is the only explicit limiting factor, and a crowding mortality term parameterizes zooplankton grazing (see methods).

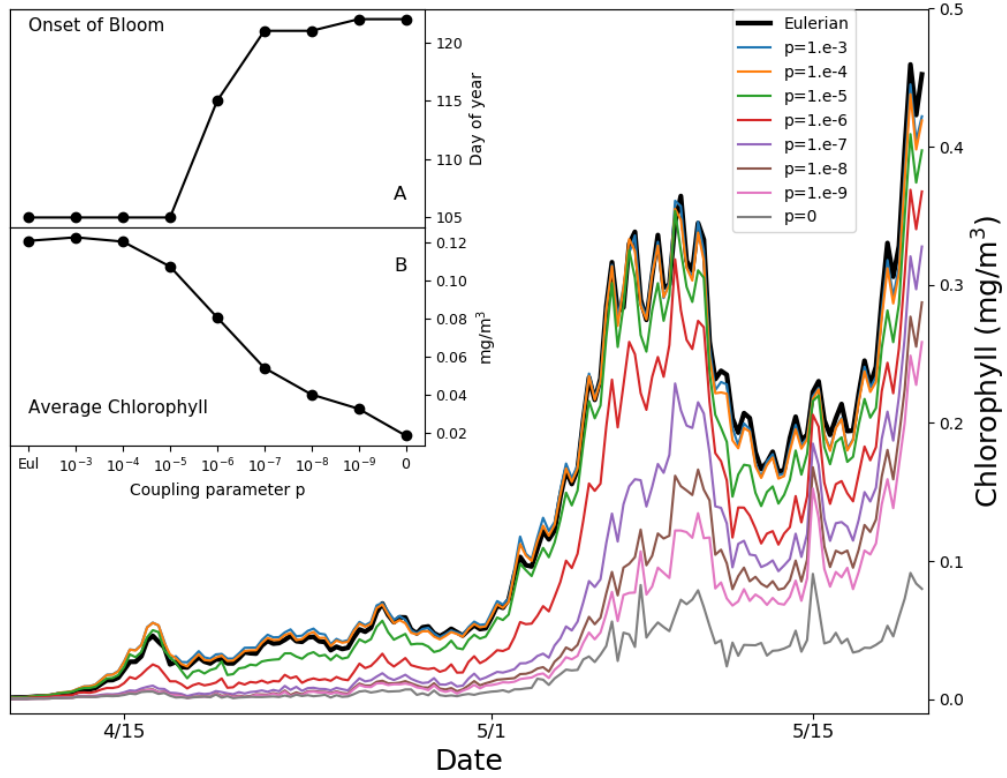


Figure 5: Average chlorophyll in the first 50 m of water column for the simulated Ocean Station PAPA in the North-West Pacific. Thin colored lines refer to aquacosc simulations coupled with varying strength  $p$ . The thick back line refers to the eddy-diffusive Eulerian model. Inset A shows the day of the onset of the bloom (see main text); inset B shows the average chlorophyll in the period April 15th to May 15th, both of them plotted as functions of the coupling parameter.

Figure 5 shows the average chlorophyll content at PAPA station over the first 50 m of water column in the weeks when the bloom starts. We define the onset of the bloom as the first day of the year when the chlorophyll content exceeds the median plus 5% of the daily chlorophyll concentration tracked over one year [56]. Reductions of the coupling strength  $p$  delay the onset by over two weeks. The results diverge from each other before the onset of stratification, from mid April until the beginning of May, when the mixed layer depth is  $\ell \approx 100$  m (supplementary Fig. S1) and the typical mixed layer eddy diffusivity is  $\kappa \approx 0.05 \text{ m}^2\text{s}^{-1}$ , yielding a value of  $\varepsilon \approx 5$  with the growth rate  $r = 2 \text{ days}^{-1}$ . This suggests that we are witnessing the same process illustrated in Figure 4, where low irreversible mixing allows the formation of high microscale patchiness, reducing bulk growth and delaying the bloom. The Lagrangian model without any coupling shows the slower growth, but this approach is unrealistic, as demonstrated above. In the following 15 days the mixed layer becomes much shallower (supplementary Fig. S1), with typical eddy diffusivity values of  $\kappa \approx 0.025 \text{ m}^2\text{s}^{-1}$ . The time scales of growth and stirring become comparable, and the vertical light gradient ceases to be a source of patchiness. Only the entrainment of phytoplankton-poor aquacosms at the base of the mixed layer continues to be a source of patchiness. Overall, the chlorophyll content averaged over the month of the bloom initiation changes by as much as a factor 6 depending on the coupling strengths (inset B in Fig. 5).

Next, we simulate the open ocean of the sub-Antarctic zone (SAZ), characterized by a mixed layer deeper than 100 m from July to October (Fig. S2). The biological model is the same as for the PAPA simulations, but, owing to

the colder water temperature, different parameter values are used, in particular the maximum photosynthetic rate is set to  $r = 0.5 \text{ days}^{-1}$  (see methods). Throughout the year, typical simulated eddy diffusivity values in the mixed layer are  $\kappa \approx 0.06 \text{ m}^2\text{s}^{-1}$ , corresponding to  $\varepsilon \approx 1$ . Here, growth is never faster than stirring, and Sverdrup’s approximation holds. Therefore, only the intermittent deepening of the mixed layer, which scoops phytoplankton-free aquacosms from the depths, contributes to the creation of patchiness in the mixed layer. In the days immediately after a sudden deepening of the mixed layer, the dynamics is reminiscent of that shown in Fig. 2 and 3, whereby a step-like initial condition first breaks down into patchiness and then is brought to vertical homogeneity with a speed determined by the intensity of the irreversible mixing. The smaller is the mixing, the slower is the destruction of variance, and the slower is the bulk growth of phytoplankton (supplementary Fig. S2). The phenological and productivity differences are not as marked as in the PAPA simulations, but we note that coarser resolution climate models with a larger impact of irreversible mixing are likely to generate greater differences and discrepancies in the bloom phenology [57].

Recent bio-optical measurements using ARGO floats from sub Antarctic zones [58] reported the presence of substantial chlorophyll variance within the hydrographic mixed layer. This was interpreted as the signature of vertical gradients of chlorophyll at the fine scales (tens of meters), which called for some mechanism incompatible with the presence of strong turbulence. In particular, it was argued that periods of storm quiescence associated with slacking turbulence would occasionally leave the mixed layer homogeneous in density, but stirred only in its uppermost part, thus allowing for growth

in the photic zone, generating a vertical gradient of chlorophyll.

In our models, slacking turbulence and vertical gradients of light definitely produce vertical gradients of chlorophyll, even when stirring is modeled as irreversible mixing (see e.g. the Eulerian simulation profiles in mid April and end of May in Fig. S1), and effects which we neglect, such as light-dependent grazing, may greatly enhance these gradients [22]. However, patchiness at the microscale is the dominant source of variance in the mixed layer. Patchiness is visually evident in the bottom panels of Fig. 6. At lower values of  $p$ , very large relative differences in the chlorophyll content of nearby aquacosms are normal even above the turbocline. This extreme variability is quantified in Fig. 7A (see supplementary Fig. S3A for the PAPA simulations), showing the monthly average of the coefficient of variation of chlorophyll (ratio of the standard deviation and the mean) computed above the turbocline depth, thus excluding the effects of slacking turbulence. In simulations with moderate and low irreversible mixing, the coefficient of variation is never negligibly small, and even when the mixed layer is deepest and the turbulence is strongest, it doesn't drop below about 0.5. As expected, the variability is larger during the Austral summer months, when turbulence is weaker than in other seasons, showing an extended peak from spring to autumn, in full agreement with the variability observed through autonomous observations in the SAZ [59]. In the Eulerian simulation, and in Lagrangian simulations with very strong irreversible mixing, the peak is small and occurs in December, when the mixed layer is the shallowest, while the coefficient of variation remains negligibly different from zero in other months.

These results, for  $p = 10^{-6}$  or lower, bear a strong resemblance to the

statistics of the ARGO float observations in the Southern Ocean (Fig. 6 in [58]), but suggest that, rather than by external forcing, chlorophyll variability is mostly caused by differences in the Lagrangian histories of water parcels [44, 30] but modulated by irreversible mixing. We remark that ARGO floats are not high-resolution chlorophyll profilers [58], and can't accurately represent vertical fluctuations on scales smaller than a few meters. The black lines in the lower panels of Fig. 6 have been computed from the aquacosm concentration using a smoothing procedure yielding 5 m of resolution (see methods), thus comparable with that of the floats. Chlorophyll fluctuations are damped, but not completely wiped out. The resolution length scale of observations affects variance estimations, as found when high-frequency sampling instruments are used [59]. In Figure 7B (Fig. S3B for PAPA) we show the monthly average of the coefficient of variation of the simulation data relative to  $p = 10^{-7}$ , after they underwent this coarse-graining procedure at several resolutions. Extreme smoothing yields estimates of fluctuations not far from those of the Eulerian simulations, which progressively increase as the resolution increases. Thus, albeit the ARGO data are surprising in the amount of variability that they show, we suspect that this is still an underestimation of the reality.

## Discussion and Conclusion

When considering mesoscale, and, more recently, submesoscale dynamics, it has often been stressed that the joint effect of turbulent stirring and nonlinear biochemical processes must produce an uneven, patchy distribution of active



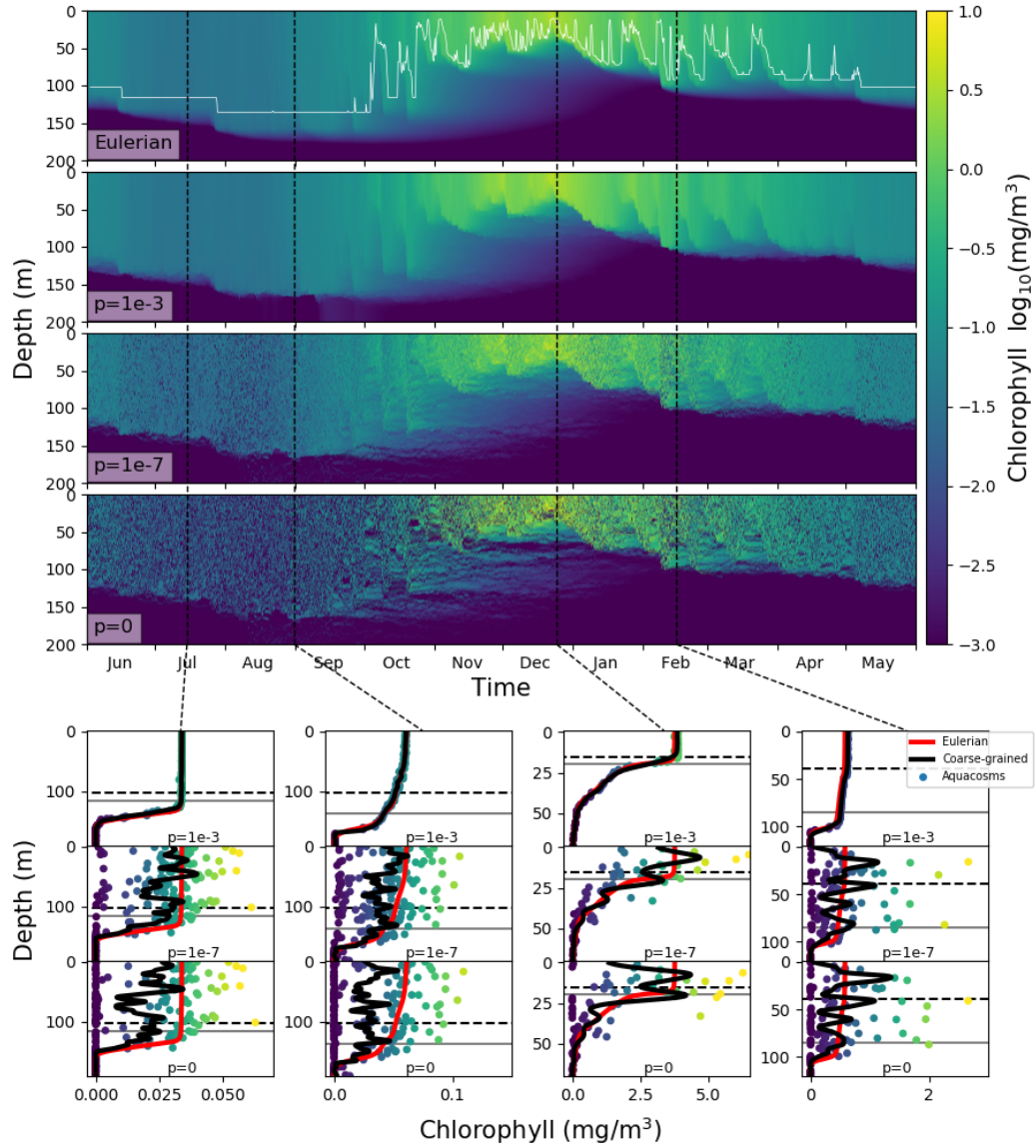


Figure 6: Top four panels: chlorophyll in the SAZ simulation in logarithmic units. The top panel shows the eddy-diffusive Eulerian model, and the thin white line marks the mixed layer depth; the next three show the aquacosm simulations for  $p = 10^{-3}, 10^{-7}, 0$ . The lower panels show, as a function of depth, the chlorophyll content in  $\text{mg/m}^3$  of the aquacosms (dots) for different values of  $p$ , their coarse-grained version (black line, see methods), the mixed layer depth (horizontal gray line) and the turbocline depth (horizontal black dashed line) at the date marked in the upper panels by the vertical black dashed lines. For comparison, the chlorophyll concentration as a function of depth computed with the Eulerian simulation (red line) is repeated in all the panels corresponding to the same date.

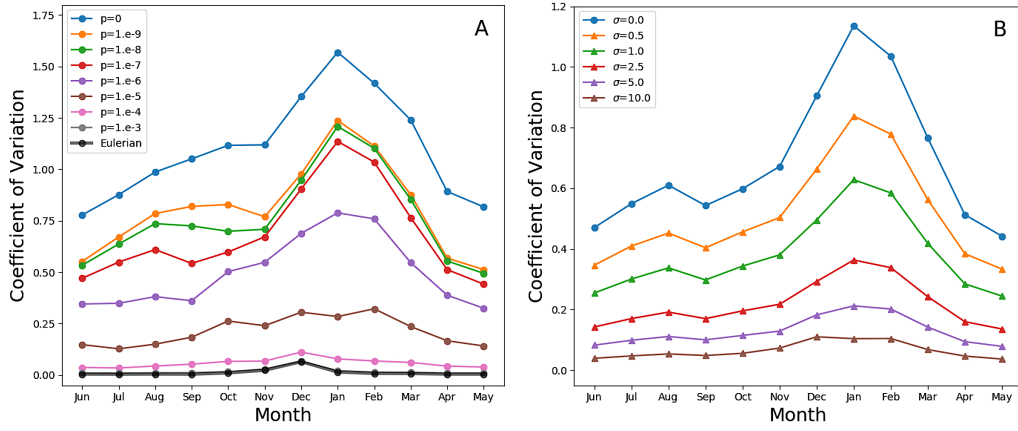


Figure 7: **A**: monthly average coefficient of variation (standard deviation over mean) of the chlorophyll above the turbocline depth in the SAZ simulation. A value of 0 indicates homogeneity, while a value of 1 implies departures from the vertical mean that are as large as the mean itself. The thin lines in color refer to the Lagrangian aquacosms with different values of the coupling parameter  $p$ . The thick black line refers to the eddy-diffusive Eulerian simulation. **B**: monthly average coefficient of variation of the Lagrangian simulation with  $p = 10^{-7}$ , and the same quantity computed from profiles coarse-grained using a Gaussian kernel estimator with standard deviation  $\sigma = 0.5, 1, 2.5, 5, 10$  m. The line  $\sigma = 0$  refers to the uncoarsened results.

tracers, and this, in turn, may affect the bulk productivity and structure of oceanic ecosystems (see [16, 60, 17, 18] and references therein). Here we remark that the fundamental idea expressed in those studies should also be scrutinized at smaller scales, e.g. across the water column.

There exists a very large body of literature on the specific problem which is the focus of this paper, namely the onset of open-ocean blooms. Some of this literature tackles the problem of how different turbulence properties affect biological growth. Yet the distinction between the time scales of turbulent stirring and the time scales of irreversible mixing is never considered. In spite of mounting evidence of ubiquitous presence of patchiness in the vertical direction across the mixed layer, theories of the onset of the bloom freely interchange turbulent stirring and irreversible mixing as if they were one and the same thing, (see the recent review [46] and references therein). On the other hand, the literature on mixed layer plankton patchiness [19, 20, 21, 22] focuses on unveiling the underlying mechanisms but does not investigate how patchiness contributes to signal at larger scales and how it should be included in predictive models. In the present work we identified two simple and distinct mechanisms that create patchiness vertically in the mixed layer, and we showed how that affects longer time scales, such as the phenology of the spring bloom. The first mechanism is essentially physical: when deeper, phytoplankton-poor water is entrained by turbulence into the phytoplankton-rich mixed layer, rapid mechanical stirring produces a highly patchy water column. The second requires the existence of a depth-dependent growth/decay process (e.g. due to the vertical gradient of light) acting on time scales faster than the stirring time scales. When this occurs, the uneven

growth at different depths creates a vertical gradient of the active tracers, which breaks down into patchiness under the action of stirring.

Eulerian models that replace unresolved stirring with irreversible mixing can't generate any patchiness from either of these mechanisms. Because the time scale of removal of the fluctuations is the same as that of stirring, (or, equivalently, because there is no way to distinguish between eddy and molecular diffusion) fluctuations around the local mean of phytoplankton and of any other tracer in the model are wiped out with extreme efficiency (Figs. 2,3,4). Recent measurements have shown that these fluctuations are large in the real ocean [51], and therefore the classical decomposition methods, such as the one proposed by [50], are insufficient to describe their nature. Lagrangian ensembles and individual-based models, where transport is described by displacing the position of the particles, produce patchiness through both mechanisms, but each particle fully preserves its individual history (there is no equivalent of molecular diffusion), so that its biochemical evolution remains completely independent from that of all the others, to the point of generating paradoxical results.

We present a modeling approach which is Lagrangian in nature, but allows for locally interacting particles; using the aquacosc concept, growth, stirring and irreversible mixing can be treated separately, as interacting but mutually independent parts of a complete biogeochemical model. Because the reaction terms are representative of the biogeochemical dynamics occurring in a very small, homogeneous water mass, they can effectively include empirical reaction norms derived from laboratory experiments and can retain the relationship with the environmental drivers as they were originally

measured [61]. In other words, our approach simulates biogeochemistry at the sub-microscale, and therefore doesn't need to deal with "effective" biological parameters or other bulk formulae as in the case of Eulerian models, contributing to unambiguously identifying the mechanistic processes which give rise to the complex phenomena occurring in plankton ecosystems. Irreversible mixing, modeled as mass fluxes between nearby aquacosms, connects the microscopic scales of the biogeochemical processes with the macroscopic ones of the physical stirring, cutting through the unresolved scales.

Aquacosm simulations are just as under resolved as Eulerian simulations having a number of mesh nodes comparable to the number of Lagrangian particles, but they treat unresolved turbulent stirring and irreversible mixing as separate and distinct processes. The time scale associated to the latter is set through the choice of the parameter  $p$ . Formally, as specified by eq. (9) in "methods",  $p$  determines the amount of the material oozed out of the  $i$ -th aquacosm that ends up being caught into the  $j$ -th within a time step. In a three-dimensional setting, this number must be interpreted as a volume (e.g.,  $p = 10^{-6}$  in a simulation using meters as unit of length would correspond to aquacosms of one cubic centimeter of volume). A better interpretation of the significance of  $p$  and of the other parameters determining the strength of the irreversible mixing (interparticle distance, time step, etc.) is developed in the supplementary material S3. There we show that the coupling between aquacosms (eq. (10) in "methods") can be associated to a diffusion coefficient, which in aquacosms simulations plays the role of molecular diffusion. We find that with the PAPA simulation parameters and  $p$  in the range between  $10^{-7}$  and  $10^{-8}$ , this coefficient assumes a value of the same order of

magnitude of the diffusivity of seawater ions, thus suggesting that this is a realistic range for those simulations.

We find that, depending on the degree of irreversible mixing, the onset of the bloom is shifted by a number of days comparable with the shifts that may occur at the end of the century [62] according to climatological models. For strengths of irreversible mixing that we consider realistic, we find a shift which would largely mitigate the problem of anticipated blooms in the Southern Ocean [57] plaguing current Eulerian models. This and other stubborn biases have often been attributed to inadequacies of the biological formulation, but are likely to stem from mismodeling the interaction, across vastly different scales, of growth and stirring, mediated by irreversible mixing [63].

Aquacosm simulations offer an ideal tool for exploring which biological features are able to build up large-scale impacts, and which are negligible in terms of bulk properties. The aquacosm approach is not limited to the extremely simplified treatment of the growth/decay processes that we have used here to illustrate the potentialities of the method, and can be expanded to include all the biogeochemical processes that may be deemed relevant for the specific problem at hand.

## Methods

### The aquacosm approach

A generic Lagrangian-ensemble water-column model is embodied by the following equations

$$dz_i = \frac{\partial}{\partial z} \kappa(z_i, t) dt + \sqrt{2\kappa(z_i, t)} dW_i \quad (7)$$

$$\begin{cases} \dot{c}_i^{(1)} &= f_1(c_i^{(1)}, \dots, c_i^{(m)}, z_i, t) \\ &\vdots \\ \dot{c}_i^{(m)} &= f_m(c_i^{(1)}, \dots, c_i^{(m)}, z_i, t) \end{cases} \quad (8)$$

where the index  $i = 1, \dots, N$  identifies the particle having depth  $z_i$ , that performs a Brownian motion characterized by an eddy diffusivity  $\kappa$ , which may depend on depth and time  $t$ ;  $W_i$  is a realization of the standard Wiener process. See [64, 65] for a derivation of equation (7). The quantities  $c_i^{(1)}, \dots, c_i^{(m)}$  are the concentrations of the  $m$  scalar quantities describing the planktonic ecosystem (e.g. in an NPZD model it would be  $m = 4$ , with concentrations of nutrient, phytoplankton, zooplankton and detritus, respectively) and the overlying dot denotes the time derivative. The functions  $f_1, \dots, f_m$  describe the reaction kinetics, where the dependence on depth and time accounts for the effect of light and its daily and seasonal variations, and for any other external forcing.

In the aquacosm approach we interpret the Lagrangian particles as tiny control volumes. They should be thought of as minuscule aquatic mesocosms

carried by the ocean dynamics, and which are homogeneous in their scalar content. This interpretation is shared with the Lagrangian-ensemble models, but, to avoid the issues discussed in the main text, we propose, in addition, to allow mass exchanges between nearby aquacosms. We define the mass fraction  $q_{ij}$  that the  $i$ -th aquacosm gives to the  $j$ -th aquacosm as

$$q_{ij} = \begin{cases} p (4\pi K_{ij} \Delta t)^{-1/2} \exp\left(-\frac{|z_i - z_j|^2}{4K_{ij} \Delta t}\right), & |z_i - z_j| < R \\ 0, & |z_i - z_j| \geq R \end{cases} \quad (9)$$

then, at intervals of time  $\Delta t$ , we update the concentrations carried by each particle as

$$c_i^{(l)} \leftarrow c_i^{(l)} - \sum_{j=1}^N q_{ij} c_i^{(l)} + \sum_{j=1}^N q_{ji} c_j^{(l)}, \quad l = 1, \dots, m \quad (10)$$

for all the scalars  $l = 1, \dots, m$ . Here the first sum represents the mass fraction that leaves the  $i$ -th aquacosm and is redistributed to all the other aquacosms, and the second sum, conversely, represents an equal mass fraction received by the  $i$ -th aquacosm from all the others (note that  $q_{ij} = q_{ji}$ ). The received mass fraction is composed of many distinct parts, each carrying the concentration of the scalars contained in the aquacosm of provenance. These parts immediately and irreversibly homogenize with the remaining content of the  $i$ -th aquacosm in order to determine its new concentration values. Here  $p$  is a free parameter, which in this one-dimensional formulation has the dimensions of a length, but in three dimensions would be a volume, that can be used to tune the coupling strength between the aquacosms (choosing



$p = 0$  is equivalent to using the a Lagrangian ensemble model with uncoupled particles). The variance of the Gaussian kernel coupling the  $i$ -th and  $j$ -th aquacosms is chosen on the basis of the eddy diffusion coefficient as

$$K_{ij} = \min \{ \kappa(z_i, t), \kappa(z_j, t) \}.$$

In order to allow for an efficient numerical implementation, the coupling between aquacosms further apart than some threshold distance  $R$  must be zero. This algorithm conserves mass and avoids the creation of spurious maxima and minima [29], provided that the parameters are chosen so that

$$\forall i, \quad \sum_{j=1}^N q_{ij} \leq 1.$$

Roughly speaking, one may think the aquacosms as oozing out part of their content into Gaussian clouds spreading at a rate specified by the eddy diffusion coefficient. Then, at regular intervals of time  $\Delta t$ , all the material within a control volume (both what was left inside the volume, and what came from the overlapping clouds) is instantaneously and irreversibly homogenized, thus determining the concentrations which will evolve according to (8) for the next interval of time  $\Delta t$ . A conceptually similar technique describing advection-diffusion processes as the interleaving of short time intervals of pure transport alternated with instantaneous irreversible mixing events has already been successfully used to model mixed layer dynamics [66]. These sort of modeling procedures have their justification rooted in the fractional step method for the numerical solution of differential equations.

All Lagrangian results presented in this paper use 200 aquacosms. Equations (7), (8) were integrated [64, 65] using Milstein’s and the midpoint methods, respectively, with a time step  $\Delta t = 10^{-5}$  non-dimensional time units for the idealized cases of Figures 2-4 and  $\Delta t = 5$  s for the PAPA and SAZ cases. The eddy diffusivity profiles for the latter cases were generated by a physical ocean model described below and were interpolated at the position of the aquacosms with monotone B-splines [67]. For simplicity, reflecting boundary conditions were imposed at 200 m of depth. The interaction radius was  $R = 0.05$  non-dimensional units for the idealized cases and  $R = 10$  m for the PAPA and SAZ simulations.

Coarse-grained profiles were obtained by smoothing the concentrations with a Gaussian kernel estimator [64] having a standard deviation of  $1/20$  of the domain for the idealized cases and 2.5 m for PAPA and SAZ, or as otherwise specified in the figure caption.

## **Eulerian models**

All the Eulerian models in this paper are solved with an explicit, second-order finite differences scheme, with  $C$  and  $\kappa$  evaluated on staggered uniform grids. The simulated water column is one non-dimensional length unit with mesh size of  $1/200$  units for the idealized cases and 200 m deep for PAPA and SAZ, with a mesh size of 1 m (see below). In all cases no-flux boundary conditions are imposed at the top and bottom of the water column. The eddy diffusivity  $\kappa$  is interpolated onto the uniform grid with the same B-spline interpolator used for the Lagrangian simulations.

## The PAPA and SAZ models

The chosen station locations are representative of two typical stratification regimes in the open ocean. Since we focused on the relationship between turbulence and light, the key distinguishing feature is the time evolution of the vertical water column structure. Weather station PAPA is located in the North-East Pacific (50°N, 145°W), and it is characterized by mixing confined to less than 100 m with maximum cooling in March-April and the development of summer stratification between June and October. The PAPA station has been used in the literature to develop and analyze turbulence closure models [68, 69]. We used a 1-D version of the NEMO physical ocean model with the parameterizations described in [69]. The model was run with 75 vertical levels and forced by ECMWF ERA-interim reanalyses [70], to obtain the hourly values of eddy diffusivity used in the Eulerian and Lagrangian biogeochemical models. A similar model was developed for the Sub-Antarctic zone of the Southern Ocean (SAZ), using the same vertical grid and same type of atmospheric forcing as in PAPA. This model site is ideally located in the Atlantic sector at 45°S 8°E, in similar light conditions as for PAPA. This region features deep mixing beyond 100 m between May and August and weak stratification during the Austral summer months.

To illustrate the versatility of the aquacosm approach to incorporate any kind of biogeochemical model with varying complexity beyond the non-dimensional study cases, we used a simplified version of the Biogeochemical Flux Model [27]. The chosen formulation tracks phytoplankton carbon concentration  $C$ , measured in  $\text{mg m}^{-3}$  for a generic functional type of mid-sized

diatoms, in which growth is only limited by light availability and an implicit temperature dependence is included in the parameter choice to account for the different oceanic regions.

The photosynthetic available radiation  $E_{PAR}$  is propagated according to the Lambert-Beer formulation

$$E_{PAR}(z) = \varepsilon_{PAR} Q_S e^{\lambda_w z + \int_z^0 \lambda_{bio}(z') dz'} \quad (11)$$

where  $Q_s$  is the net broadband solar radiation at the surface from ERA-interim ( $\text{W m}^{-2}$ ),  $\varepsilon_{PAR} = 0.4/0.217$  is the coefficient determining the fraction of photosynthetically-available radiation (converted to  $\mu\text{E m}^{-2}\text{s}^{-1}$  using the constant 0.217). Light propagation takes into account the extinction due to pure water  $\lambda_w$  ( $0.0435 \text{ m}^{-1}$ ) and to phytoplankton concentration  $\lambda_{bio}$ . The broadband biological light extinction is approximated to a linear function of the phytoplankton chlorophyll concentration  $L$

$$\lambda_{bio} = cL \quad (12)$$

regulated by the specific absorption coefficient ( $c = 0.03 \text{ m}^2 \text{ mg chl}^{-1}$ ). To be more comparable with the non-dimensional idealized experiments, this very simple model neglects photoacclimation phenomena, therefore we assume

$$L = \theta_{chl} C \quad (13)$$

where the chlorophyll to carbon ratio  $\theta_{chl}$  was taken to be  $0.017 \text{ mg chl mg } C^{-1}$  for PAPA and  $0.013$  for SAZ [71, 72]. The same results (not shown)

were confirmed using the BFM acclimation model with variable chlorophyll, based on the Geider et al. formulation [73, 27]. The carbon concentration rate of change is controlled by gross primary production, respiration and a crowding mortality term that parameterizes zooplankton grazing:

$$\dot{C} = rf^EC - bC - \frac{aC^2}{C_h + C} \quad (14)$$

where  $r$  is the maximum specific photosynthetic rate,  $b$  is the basal specific respiration rate,  $a$  is the specific crowding mortality rate and  $C_h$  is the crowding half-saturation. Owing to the difference in the seasonal cycle of nutrients and water temperature, we use  $r = 2$ ,  $b = 0.16$ ,  $a = 1 \text{ days}^{-1}$  for PAPA and  $r = 0.5$ ,  $b = 0.04$ ,  $a = 0.25 \text{ days}^{-1}$  for SAZ. The lower potential growth rate in SAZ is derived by applying a Q10 relationship [27] and considering the mean temperature during the bloom period. The other parameters are tuned to yield realistic values of chlorophyll at the study sites. In all cases we set  $C_h = 12.5 \text{ mg m}^{-3}$ . The light regulating factor is defined as

$$f^E = 1 - \exp\left(-\frac{\alpha E_{PAR}}{r}\theta_{chl}\right) \quad (15)$$

where  $\alpha = 1.38 \cdot 10^{-5} \text{ } \mu\text{E}^{-1}\text{m}^2$  [27].

The eddy-diffusive Eulerian version of this model is

$$\frac{\partial C}{\partial t} = \frac{\partial}{\partial z} \left( \kappa(z, t) \frac{\partial C}{\partial z} \right) + \dot{C}. \quad (16)$$

The Lagrangian aquacosc models use  $m = 1$  and (8) reduces to (14).

Starting from initial conditions having a small constant concentration,

the runs extend for four years (each year repeats the same eddy diffusivity and radiation data). Except for the first year, in all models the results have negligible differences between the years.

## References

- [1] Azam, F. & Worden, A. Z. Microbes, Molecules, and Marine Ecosystems. *Science* **303**, 1622–1624 (2004). URL <http://science.sciencemag.org/content/303/5664/1622>. 15016987.
- [2] Legendre, L., Rivkin, R. B. & Jiao, N. Advanced experimental approaches to marine water-column biogeochemical processes. *ICES J Mar Sci* **75**, 30–42 (2018). URL <https://academic.oup.com/icesjms/article/75/1/30/4080730>.
- [3] Gruber, N. *et al.* Oceanic sources, sinks, and transport of atmospheric CO<sub>2</sub>. *Global Biogeochemical Cycles* **23**, GB1005 (2009).
- [4] Bopp, L. *et al.* Multiple stressors of ocean ecosystems in the 21st century: Projections with CMIP5 models. *Biogeosciences* **10**, 6225–6245 (2013).
- [5] Piroddi, C. *et al.* Using ecological models to assess ecosystem status in support of the European Marine Strategy Framework Directive. *Ecological Indicators* **58**, 175–191 (2015). URL <http://www.sciencedirect.com/science/article/pii/S1470160X1500285X>.
- [6] Hyder, K. *et al.* Making modelling count - increasing the contribution of shelf-seas community and ecosystem models to policy development and

- management. *Marine Policy* **61**, 291–302 (2015). URL <http://www.sciencedirect.com/science/article/pii/S0308597X1500216X>.
- [7] Travers, M., Shin, Y. J., Jennings, S. & Cury, P. Towards end-to-end models for investigating the effects of climate and fishing in marine ecosystems. *Progress in Oceanography* **75**, 751–770 (2007). URL <http://www.sciencedirect.com/science/article/pii/S0079661107001425>.
- [8] Fu, C. *et al.* Risky business: The combined effects of fishing and changes in primary productivity on fish communities. *Ecological Modelling* **368**, 265–276 (2018). URL <http://www.sciencedirect.com/science/article/pii/S0304380017302661>.
- [9] Stec, K. F. *et al.* Modelling plankton ecosystems in the meta-omics era. Are we ready? *Marine Genomics* **32**, 1–17 (2017). URL <http://www.sciencedirect.com/science/article/pii/S1874778716301544>.
- [10] Denman, K. L. Modelling planktonic ecosystems: Parameterizing complexity. *Progress in Oceanography* **57**, 429–452 (2003). URL <http://www.sciencedirect.com/science/article/pii/S0079661103001095>.
- [11] Tian, R. C. Toward standard parameterizations in marine biological modeling. *Ecological Modelling* **193**, 363–386 (2006). URL <http://www.sciencedirect.com/science/article/pii/S0304380005004473>.
- [12] Nihoul, J. C. *Modelling of marine systems*, vol. 10 of *Elsevier Oceanography Series* (Elsevier, 1975).

- [13] Nihoul, J. C. J. & Djenidi, S. Coupled physical and biological models. In Brink, K. H. & Robinson, A. R. (eds.) *The Sea*, vol. 10, 483–506 (John Wiley & Sons, Inc., 1998).
- [14] Pinel-Alloul, B. & Ghadouani, A. Spatial Heterogeneity Of Planktonic Microorganisms In Aquatic Systems. In Franklin, R. B. & Mills, A. L. (eds.) *The Spatial Distribution of Microbes in the Environment*, 203–310 (Springer Netherlands, 2007). URL [https://doi.org/10.1007/978-1-4020-6216-2\\_8](https://doi.org/10.1007/978-1-4020-6216-2_8).
- [15] Prairie, J. C., Sutherland, K. R., Nickols, K. J. & Kaltenberg, A. M. Biophysical interactions in the plankton: A cross-scale review. *Limnology and Oceanography: Fluids and Environments* **2**, 121–145 (2012). URL <https://aslopubs.onlinelibrary.wiley.com/doi/abs/10.1215/21573689-1964713>.
- [16] Martin, A. P. Phytoplankton patchiness: The role of lateral stirring and mixing. *Progress in Oceanography* **57**, 125–174 (2003). URL <http://www.sciencedirect.com/science/article/pii/S0079661103000855>.
- [17] Mahadevan, A. The Impact of Submesoscale Physics on Primary Productivity of Plankton. *Annual Review of Marine Science* **8**, 161–184 (2016). URL <https://doi.org/10.1146/annurev-marine-010814-015912>. 26394203.
- [18] Lévy, M., Franks, P. J. S. & Smith, K. S. The role of submesoscale currents in structuring marine ecosystems. *Nature Communi-*



- cations* **9**, 4758 (2018). URL <https://www.nature.com/articles/s41467-018-07059-3>.
- [19] Huisman, J., Pham Thi, N. N., Karl, D. M. & Sommeijer, B. Reduced mixing generates oscillations and chaos in the oceanic deep chlorophyll maximum. *Nature* **439**, 322–325 (2006). 16421570.
- [20] Durham, W. M. & Stocker, R. Thin Phytoplankton Layers: Characteristics, Mechanisms, and Consequences. *Annu. Rev. Mar. Sci.* **4**, 177–207 (2011). URL <http://www.annualreviews.org/doi/10.1146/annurev-marine-120710-100957>.
- [21] Cullen, J. J. Subsurface Chlorophyll Maximum Layers: Enduring Enigma or Mystery Solved? *Annual Review of Marine Science* **7**, 207–239 (2015). URL <https://doi.org/10.1146/annurev-marine-010213-135111>. 25251268.
- [22] Moeller, H. V., Laufkötter, C., Sweeney, E. M. & Johnson, M. D. Light-dependent grazing can drive formation and deepening of deep chlorophyll maxima. *Nature Communications* **10**, 1978 (2019). URL <https://www.nature.com/articles/s41467-019-09591-2>.
- [23] Foloni-Neto, H., Tanaka, M., Joshima, H. & Yamazaki, H. A comparison between quasi-horizontal and vertical observations of phytoplankton microstructure. *J Plankton Res* **38**, 993–1005 (2016). URL <https://academic.oup.com/plankt/article/38/4/993/2451708>.
- [24] Currie, W. J. S. & Roff, J. C. Plankton are not passive tracers: Plankton in a turbulent environment. *Journal of Geophysical Research: Oceans*

- (2006). URL <https://agupubs.onlinelibrary.wiley.com/doi/abs/10.1029/2005JC002967>.
- [25] Doubell, M. J., Yamazaki, H., Li, H. & Kokubu, Y. An advanced laser-based fluorescence microstructure profiler (TurboMAP-L) for measuring bio-physical coupling in aquatic systems. *J Plankton Res* **31**, 1441–1452 (2009). URL <https://academic.oup.com/plankt/article/31/12/1441/1503781>.
- [26] Le Quéré, C. *et al.* Ecosystem dynamics based on plankton functional types for global ocean biogeochemistry models. *Global Change Biology* **11**, 2016–2040 (2005).
- [27] Vichi, M., Pinardi, N. & Masina, S. A generalized model of pelagic biogeochemistry for the global ocean ecosystem. Part I: Theory. *Journal of Marine Systems* **64**, 89–109 (2007).
- [28] Aumont, O., Ethé, C., Tagliabue, A., Bopp, L. & Gehlen, M. PISCES-v2: An ocean biogeochemical model for carbon and ecosystem studies. *Geoscientific Model Development* **8**, 2465–2513 (2015).
- [29] Paparella, F. & Popolizio, M. Lagrangian numerical methods for ocean biogeochemical simulations. *Journal of Computational Physics* **360**, 229–246 (2018). URL <http://www.sciencedirect.com/science/article/pii/S002199911830041X>.
- [30] Baudry, J., Dumont, D. & Schloss, I. R. Turbulent mixing and phytoplankton life history: A Lagrangian versus Eulerian model com-

- parrison.
- Marine Ecology Progress Series*
- 600**
- , 55–70 (2018). URL
- <https://www.int-res.com/abstracts/meps/v600/p55-70/>
- .
- [31] Woods, J. D. & Onken, R. Diurnal variation and primary production in the ocean preliminary results of a Lagrangian ensemble model. *J Plankton Res* **4**, 735–756 (1982). URL <https://academic.oup.com/plankt/article/4/3/735/1486449>.
- [32] Wolf, K. U. & Woods, J. D. Lagrangian Simulation of Primary Production in the Physical Environment — The Deep Chlorophyll Maximum and Nutricline. In Rothschild, B. J. (ed.) *Toward a Theory on Biological-Physical Interactions in the World Ocean*, NATO ASI Series, 51–70 (Springer Netherlands, 1988).
- [33] Woods, J. D. *et al.* Simulating plankton ecosystems by the Lagrangian Ensemble method. *Philosophical Transactions of the Royal Society of London. Series B: Biological Sciences* **343**, 27–31 (1994). URL <http://royalsocietypublishing.org/doi/10.1098/rstb.1994.0004>.
- [34] Woods, J. D. The Lagrangian Ensemble metamodel for simulating plankton ecosystems. *Progress in Oceanography* **67**, 84–159 (2005). URL <http://www.sciencedirect.com/science/article/pii/S0079661105000893>.
- [35] Cianelli, D., Uttieri, M. & Zambianchi, E. Individual based modelling of planktonic organisms. In *Ecological Modeling*, 83–96 (2012).
- [36] Yamazaki, H. & Kamykowski, D. The vertical trajectories of motile phytoplankton in a wind-mixed water column. *Deep Sea Research Part*

- A. Oceanographic Research Papers* **38**, 219–241 (1991). URL <http://www.sciencedirect.com/science/article/pii/019801499190081P>.
- [37] Kamykowski, D., Yamazaki, H. & Janowitz, G. S. A Lagrangian model of phytoplankton photosynthetic response in the upper mixed layer. *J Plankton Res* **16**, 1059–1069 (1994). URL <https://academic.oup.com/plankt/article/16/8/1059/1468322>.
- [38] Scheffer, M., Baveco, J. M., DeAngelis, D. L., Rose, K. A. & van Nes, E. H. Super-individuals a simple solution for modelling large populations on an individual basis. *Ecological Modelling* **80**, 161–170 (1995). URL <http://www.sciencedirect.com/science/article/pii/030438009400055M>.
- [39] Hellweger, F. L. & Kianirad, E. Accounting for Intrapopulation Variability in Biogeochemical Models Using Agent-Based Methods. *Environ. Sci. Technol.* **41**, 2855–2860 (2007). URL <https://doi.org/10.1021/es062046j>.
- [40] Hellweger, F. L. & Bucci, V. A bunch of tiny individuals—Individual-based modeling for microbes. *Ecological Modelling* **220**, 8–22 (2009). URL <http://www.sciencedirect.com/science/article/pii/S0304380008004390>.
- [41] Dippner, J. W. Competition between different groups of phytoplankton for nutrients in the southern North Sea. *Journal of Marine Systems* **14**, 181–198 (1998). URL <http://www.sciencedirect.com/science/article/pii/S0924796397000250>.

- [42] Lande, R. & Lewis, M. R. Models of photoadaptation and photosynthesis by algal cells in a turbulent mixed layer. *Deep Sea Research Part A. Oceanographic Research Papers* **36**, 1161–1175 (1989). URL <http://www.sciencedirect.com/science/article/pii/0198014989900988>.
- [43] McGillicuddy, D. J. One-dimensional numerical simulation of primary production: Lagrangian and Eulerian formulations. *J Plankton Res* **17**, 405–412 (1995). URL <https://academic.oup.com/plankt/article/17/2/405/1490010>.
- [44] Kida, S. & Ito, T. A lagrangian view of spring phytoplankton blooms. *Journal of Geophysical Research: Oceans* **122**, 9160–9175 (2017).
- [45] Sverdrup, H. V. On conditions for the vernal blooming of phytoplankton. *J. Cons. Perm. Int. Exp. Mer* **18**, 287–295 (1953).
- [46] Fischer, A. *et al.* Sixty Years of Sverdrup: A Retrospective of Progress in the Study of Phytoplankton Blooms. *Oceanography* **27**, 222–235 (2014). URL <https://tos.org/oceanography/article/sixty-years-of-sverdrup-a-retrospective-of-progress-in-the-study-of-phytopl>
- [47] Sathyendranath, S., Ji, R. & Browman, H. I. Revisiting Sverdrup’s critical depth hypothesis. *ICES J Mar Sci* **72**, 1892–1896 (2015). URL <https://academic.oup.com/icesjms/article/72/6/1892/927499>.
- [48] Fennel, W. & Neumann, T. The mesoscale variability of nutrients and plankton as seen in a coupled model. *Germ. J. Hydrog.* **48**, 49–71 (1996).

- [49] Wallhead, P. J., Martin, A. P., Srokosz, M. A. & Fasham, M. J. Accounting for unresolved spatial variability in marine ecosystems using time lags. *Journal of Marine Research* **64**, 881–914 (2006).
- [50] Mandal, S. *et al.* A 1D physical–biological model of the impact of highly intermittent phytoplankton distributions. *J Plankton Res* **38**, 964–976 (2016). URL <https://academic.oup.com/plankt/article/38/4/964/2451728>.
- [51] Doubell, M. J., Prairie, J. C. & Yamazaki, H. Millimeter scale profiles of chlorophyll fluorescence: Deciphering the microscale spatial structure of phytoplankton. *Deep Sea Research Part II: Topical Studies in Oceanography* **101**, 207–215 (2014).
- [52] Huisman, J., van Oostveen, P. & Weissing, F. J. Critical depth and critical turbulence: two different mechanisms for the development of phytoplankton blooms. *Limnology and oceanography* **44**, 1781–1787 (1999).
- [53] Taylor, J. R. & Ferrari, R. Shutdown of turbulent convection as a new criterion for the onset of spring phytoplankton blooms. *Limnology and Oceanography* **56**, 2293–2307 (2011).
- [54] Ferrari, R., Merrifield, S. T. & Taylor, J. R. Shutdown of convection triggers increase of surface chlorophyll. *Journal of Marine Systems* **147**, 116–122 (2015).
- [55] Esposito, S., Botte, V., Iudicone, D. & Ribera d’Alcala’, M. Numerical analysis of cumulative impact of phytoplankton photoresponses to

- light variation on carbon assimilation. *Journal of Theoretical Biology* **261**, 361–371 (2009). URL <http://www.sciencedirect.com/science/article/pii/S0022519309003476>.
- [56] Racault, M.-F., Le Quéré, C., Buitenhuis, E., Sathyendranath, S. & Platt, T. Phytoplankton phenology in the global ocean. *Ecological Indicators* **14**, 152–163 (2012).
- [57] Hague, M. & Vichi, M. A Link Between CMIP5 Phytoplankton Phenology and Sea Ice in the Atlantic Southern Ocean. *Geophysical Research Letters* **45**, 6566–6575 (2018). URL <https://agupubs.onlinelibrary.wiley.com/doi/abs/10.1029/2018GL078061>.
- [58] Carranza, M. M. *et al.* When Mixed Layers Are Not Mixed. Storm-Driven Mixing and Bio-optical Vertical Gradients in Mixed Layers of the Southern Ocean. *Journal of Geophysical Research: Oceans* **123**, 7264–7289 (2018). URL <http://agupubs.onlinelibrary.wiley.com/doi/full/10.1029/2018JC014416>.
- [59] Little, H. J., Vichi, M., Thomalla, S. J. & Swart, S. Spatial and temporal scales of chlorophyll variability using high-resolution glider data. *Journal of Marine Systems* **187**, 1–12 (2018). URL <http://www.sciencedirect.com/science/article/pii/S0924796317304530>.
- [60] Levy, M. & Martin, A. P. The influence of mesoscale and submesoscale heterogeneity on ocean biogeochemical reactions. *Global Biogeochemical Cycles* **27**, 1139–1150 (2013). URL <http://agupubs.onlinelibrary.wiley.com/doi/full/10.1002/2012GB004518>.

- [61] Boyd, P. W. *et al.* Experimental strategies to assess the biological ramifications of multiple drivers of global ocean change: A review. *Global Change Biology* **24**, 2239–2261 (2018).
- [62] Henson, S. A., Cole, H. S., Hopkins, J., Martin, A. P. & Yool, A. Detection of climate change–driven trends in phytoplankton phenology. *Global Change Biology* **24**, e101–e111 (2018).
- [63] McKiver, W. J., Vichi, M., Lovato, T., Storto, A. & Masina, S. Impact of increased grid resolution on global marine biogeochemistry. *Journal of Marine Systems* **147**, 153–168 (2015).
- [64] Gräwe, U. Implementation of high–order particle–tracking schemes in a water column model. *Ocean Modelling* **36**, 80–89 (2011).
- [65] Van Sebille, E. *et al.* Lagrangian ocean analysis: Fundamentals and practices. *Ocean Modelling* **121**, 49–75 (2018).
- [66] Ferrari, R. & Young, W. On the development of thermohaline correlations as a result of nonlinear diffusive parameterizations. *Journal of marine research* **55**, 1069–1101 (1997).
- [67] Ross, O. N. & Sharples, J. Recipe for 1–d lagrangian particle tracking models in space–varying diffusivity. *Limnology and Oceanography: Methods* **2**, 289–302 (2004).
- [68] Burchard, H. & K., B. Comparative analysis of four second–moment turbulence closure models for the oceanic mixed layer. *J. Phys. Oceanogr.* **31**, 1943–1967 (2001).



- [69] Refray, G., Bourdalle-Badie, R. & Calone, C. Modelling turbulent vertical mixing sensitivity using a 1-D version of NEMO. *Geoscientific Model Development* **8**, 69–86 (2015).
- [70] Dee, D. P. *et al.* The ERA-Interim reanalysis: Configuration and performance of the data assimilation system. *Quarterly Journal of the Royal Meteorological Society* **137**, 553–597 (2011). URL <http://rmets.onlinelibrary.wiley.com/doi/abs/10.1002/qj.828>.
- [71] Behrenfeld, M. J., Boss, E., Siegel, D. A. & Shea, D. M. Carbon-based ocean productivity and phytoplankton physiology from space. *Global Biogeochemical Cycles* **19** (2005).
- [72] Thomalla, S. J., Ogunkoya, A. G., Vichi, M. & Swart, S. Using Optical Sensors on Gliders to Estimate Phytoplankton Carbon Concentrations and Chlorophyll-to-Carbon Ratios in the Southern Ocean. *Frontiers in Marine Science* **4**, 34 (2017).
- [73] Geider, R. J., MacIntyre, H. L. & Kana, T. M. A dynamic model of phytoplankton growth and acclimation: Responses of the balanced growth rate and chlorophyll a:carbon ratio to light, nutrient limitation and temperature. *Marine Ecology Progress Series* **148**, 187–200 (1997).

## Supplementary materials

### S1: On the equivalence of the Eulerian and Lagrangian approaches in Sverdrup's theory.

When the concentration  $C \ll 1$  the equation (5) may be linearized to

$$\frac{\partial C}{\partial t} = \varepsilon f(z)C + \frac{\partial^2 C}{\partial z^2} \quad (\text{S1})$$

Following Sverdrup, we consider the case of very vigorous stirring, that is  $\varepsilon \ll 1$ . Then, because the diffusion term is the dominant one, one contends that the plankton field  $C$  will be nearly independent of  $z$ , except, possibly, for an initial transient lasting no more than the mixing time scale. Thus, on integrating the above equation over the vertical domain, and exploiting the no-flux boundary conditions in the diffusion term, the time evolution of the water-column averaged phytoplankton concentration  $\langle C \rangle$  is found to evolve approximately according to

$$\frac{d}{dt} \langle C \rangle = \varepsilon I \langle C \rangle \quad (\text{S2})$$

whose solution is

$$\langle C \rangle (t) = \langle C \rangle (0) e^{\varepsilon I t}. \quad (\text{S3})$$

The sign of the constant

$$I = \int_0^1 f(z) dz \quad (\text{S4})$$

determines whether the plankton population, overall, will grow or decay. Using Sverdrup's form (4) for  $f$ , one readily recognizes that growth is possible only if the mixed layer depth  $\ell$  is not too deep with respect to the length scale  $\lambda$ .

In Lagrangian-ensemble models, a fluid parcel having depth  $z_i$  carries a homogeneous concentration  $C_i$  of phytoplankton. The trajectories of the fluid particles are generally modeled as sample paths of a Brownian motion. Regardless of the details of how their trajectory is modeled, a really important underlying hypothesis (most often not explicitly stated) is that the following ergodic identity holds

$$\lim_{t \rightarrow \infty} \frac{1}{t} \int_0^t f(z_i(\tau)) d\tau = \int_0^1 f(z) dz \quad (\text{S5})$$

where the identity must be valid for any possible choice of  $f$  and for all fluid parcels  $z_i$  (except, at most, for a set of measure zero). Namely, the time average of the value of  $f$  experienced by the typical fluid parcel along its trajectory must converge to the spatial average of  $f$ , which is the constant  $I$  appearing in (S2). The concentration of plankton carried by each particle is assumed to evolve according to the same reaction kinetics as in the Eulerian case. This leads to the following equation for each fluid parcel

$$\frac{d}{dt} C_i = \varepsilon f(z_i(t)) C_i.$$

Separating the variables, and integrating in time, we have

$$\int_{C_i(0)}^{C_i(t)} \frac{dC_i}{C_i} = \varepsilon \int_0^t f(z_i(\tau)) d\tau \quad (\text{S6})$$

If the stirring time scale, as quantified by the eddy diffusion coefficient, is much shorter than the physiological phytoplankton growth time scale, then one may contend that the ergodic identity (S5) will be approximately true not just in the limit  $t \rightarrow \infty$ , but also after any finite time  $t$  longer than the mixing time scale. Therefore, one substitutes the integral in the right-hand side of (S6) with  $I$  and finds the following approximate solution

$$C_i(t) = C_i(0)e^{\varepsilon I t} \quad (\text{S7})$$

If one tracks  $N$  Lagrangian particles, uniformly seeded along the water column, then the arithmetic average of their plankton concentration

$$\overline{C}^N(t) \equiv \frac{1}{N} \sum_{i=1}^N C_i(t) = \overline{C}^N(0) e^{\varepsilon I t}$$

will converge to Sverdrup's Eulerian solution (S3) in the limit  $N \rightarrow \infty$ .

Even though in Sverdrup's model the Lagrangian and Eulerian approaches yield identical results, this does not generalize to nonlinear cases. For instance, if we use the logistic growth model

$$\frac{\partial C}{\partial t} = \varepsilon f(z) C (1 - C) + \frac{\partial^2 C}{\partial z^2} \quad (\text{S8})$$

with the same hypothesis and approximations as in Sverdrup's model, we

find the Eulerian solution

$$\langle C \rangle(t) = \frac{\langle C \rangle(0) e^{\epsilon I t}}{\langle C \rangle(0) (e^{\epsilon I t} - 1) + 1} \quad (\text{S9})$$

where  $\langle C \rangle(0)$  is the average plankton concentration of the initial condition.

The Lagrangian model yields, along each particle

$$C_i(t) = \frac{C_i(0) e^{\epsilon I t}}{C_i(0) (e^{\epsilon I t} - 1) + 1}. \quad (\text{S10})$$

The arithmetic average of (S10) over  $N$  Lagrangian particles does not converge to the Eulerian solution (S9) in the limit  $N \rightarrow \infty$ . For example, take an initial condition containing only, and in equal proportions, fluid parcels with either  $C_i(0) = 1$  or  $C_i(0) = 0$ . Then, the arithmetic average of (S10) is:

$$\overline{C}^N(t) = \frac{1}{2}. \quad (\text{S11})$$

With the Eulerian approach, starting from  $\langle C \rangle(0) = 1/2$ , (S9) describes growing population that reaches  $\langle C \rangle = 1$  asymptotically in time. The Lagrangian and the Eulerian approaches give irreconcilably different results.

## S2: Growth rates in weak turbulence

Sverdrup's model yields an accurate approximation of the solution of equation (S1) when  $\varepsilon$  is no larger than one, that is, when the reaction time scales are no faster than the stirring time scales, as quantified by the eddy diffusion coefficient. In the opposite case, it is inappropriate to assume that turbu-

lence is able to maintain a nearly constant concentration of plankton in the water column: plankton will be more abundant close to the surface than at depth, and this results in a faster growth rate than predicted by Sverdrup's theory. In order to estimate the growth rate, we seek solutions of (S1) of the form

$$C(z, t) = A_n(t)\phi_n(z).$$

Separating the variables, one obtains:

$$A_n(t) = A_n(0) \exp(\sigma_n t)$$

where the growth rate  $\sigma_n$  is determined by seeking a non-zero solution  $\phi_n$  of the eigenvalue problem

$$\phi_n'' + \varepsilon f \phi_n = \sigma_n \phi_n \tag{S12}$$

where  $\phi_n$  is subject to the same boundary conditions as  $C$  (no-flux in our case). Sturm-Liouville theory (see, e.g. [S1]) insures the existence of a countably infinite set of pairs  $(\sigma_n, \phi_n)$ , with  $\sigma_n$  ordered and decreasing with  $n$ . The Rayleigh quotient associated to the problem (S12) is

$$q(\psi) = \frac{\varepsilon \int_0^1 f \psi^2 dz - \int_0^1 (\psi')^2 dz}{\int_0^1 \psi^2 dz} \tag{S13}$$

On multiplying (S12) by  $\phi_n$  and integrating by parts, it is easy to verify that setting  $\psi = \phi_n$  gives  $q(\psi) = \sigma_n$ . Among all non-zero, differentiable functions  $\psi$ , the one which maximizes the quotient is  $\phi_0$ . A simple, explicit form for  $\phi_0$  can not, in general, be obtained. However, using a physically motivated

choice for  $\psi$  in the Rayleigh quotient, we can still seek an approximation from below of the value of  $\sigma_0$ , which is the growth rate that we expect to observe in a solution of equation (S1) starting from initial conditions very close to zero.

Sverdrup's theory uses the approximation  $\phi_0(z) \approx \psi(z) = 1$ , which yields the following estimate for the growth rate

$$\sigma_0 \approx q(\psi) = \varepsilon \int_0^1 f(z) dz$$

as in equation (S1). This is an appropriate maximization strategy for small  $\varepsilon$ : when the first integral at the numerator of (S13) is multiplied by a tiny number, then the second integral must be kept small by maintaining  $\psi'$  very close to zero in order to obtain the largest possible value of  $q$ . In the case of weak turbulence, that is, for large  $\varepsilon$ , the plankton residing in the sunlit region close to the surface has time to grow before being fluxed down in the dark depths. Therefore, the presence of a vertical plankton concentration gradient is expected, and a functional form such as

$$\psi_\alpha = 1 + \alpha \cos(\pi z) \tag{S14}$$

will give a better approximation than Sverdrup's, if the value of the constant  $\alpha$  is chosen appropriately. Using the *ansatz* (S14) in (S13) results in the following quotient

$$q(\psi_\alpha) = \frac{\varepsilon (2I + 4\alpha I_1 + 2\alpha^2 I_2) - \pi^2 \alpha^2}{\alpha^2 + 2} \tag{S15}$$

where the Sverdrup integral  $I$  is given in (S4), and we defined

$$I_1 = \int_0^1 f(z) \cos(\pi z) dz; \quad I_2 = \int_0^1 f(z) \cos^2(\pi z) dz.$$

As is verifiable by analytical means, the value of  $q$  in (S15) has a single maximum attained for positive  $\alpha$ . For small  $\varepsilon$  such a maximum is nearly indistinguishable from the value attained for  $\alpha = 0$ , but, as  $\varepsilon$  increases, the difference becomes sizable. In particular, for  $\epsilon = 10$  we have  $q(\psi_0) = 0.498 \dots$ , and  $q(\psi_{\alpha_{max}}) = 0.820 \dots$ . The latter value is the growth rate used to plot the thin solid line in Figure 4, showing, as expected, just a slight underestimation of the growth rates observed both in the Eulerian and in the Lagrangian simulations, in the linear regime.

### **S3: Strength of the irreversible mixing**

In order to evaluate the effects of the coupling formula (10), so as to give guidance in choosing a realistic value for the parameter  $p$ , it is convenient to consider the hypothetical case in which the eddy diffusivity is a constant  $K$ , and the aquacosms are arranged along the water column at equally spaced depths  $z_i = ih$ . If one chooses an interaction length  $R$  such that the  $i$ -th aquacosm interacts only with the  $(i - 1)$ -th and the  $(i + 1)$ -th then, (10) in the main text becomes

$$c^{(l)}(z_i, t + \Delta t) = c^{(l)}(z_i, t) - 2qc^{(l)}(z_i, t) + qc^{(l)}(z_{i+1}, t) + qc^{(l)}(z_{i-1}, t)$$



where

$$q = \frac{p}{(4\pi K \Delta t)} \exp\left(-\frac{h^2}{4K \Delta t}\right).$$

This can be re-arranged as

$$\frac{c^{(l)}(z_i, t + \Delta t) - c^{(l)}(z_i, t)}{\Delta t} = \frac{h^2}{\Delta t} q \left( \frac{c^{(l)}(z_{i+1}, t) + c^{(l)}(z_{i-1}, t) - 2c^{(l)}(z_i, t)}{h^2} \right)$$

which is the forward in time, centered in space finite difference method for the diffusion equation associated to the diffusion coefficient

$$\mathcal{D} = \frac{h^2}{\Delta t} q. \tag{S16}$$

Because equation (10) represents the irreversible mixing processes, it is legitimate to interpret  $\mathcal{D}$  as a molecular diffusion coefficient. For actual simulations where the particles are scattered at uniformly random depths, the expression (S16) can still be used as a guidance, provided that  $h$  is interpreted as the mean distance between first neighbors. When the value of  $R$  is such that more than three aquacosms interact simultaneously, it is natural to expect a somewhat larger diffusivity, because each aquacosm exchanges more mass with other aquacosms, but if  $R > \sqrt{2K\Delta t}$ , this effect will be less than proportional to the number of particles, because aquacosms substantially further away than  $\sqrt{2K\Delta t}$  contribute very little [29].

For the PAPA simulations  $K \approx 0.025 \text{ m}^2\text{s}^{-1}$ ,  $h = 1 \text{ m}$ ,  $\Delta t = 5 \text{ s}$ . We also have  $R = 10 \text{ m}$ , so that, on average, 20 aquacoms are simultaneously interacting, and  $\sqrt{2K\Delta t} = 0.5 \text{ m}$ . On choosing  $p = 10^{-7}$  we obtain  $\mathcal{D} \approx 2 \cdot 10^{-9} \text{ m}^2\text{s}^{-1}$ . Considering that the molecular diffusivity of ions in seawater

is of the order of  $10^{-9} \text{ m}^2\text{s}^{-1}$ , it seems reasonable to assume that realistic values for  $p$  should range between  $10^{-8}$  and  $10^{-7}$ .

## Supplementary References

- [S1] Strauss, W. A. *Partial differential equations: An introduction*. John Wiley & Sons (2007).

## Supplementary figures

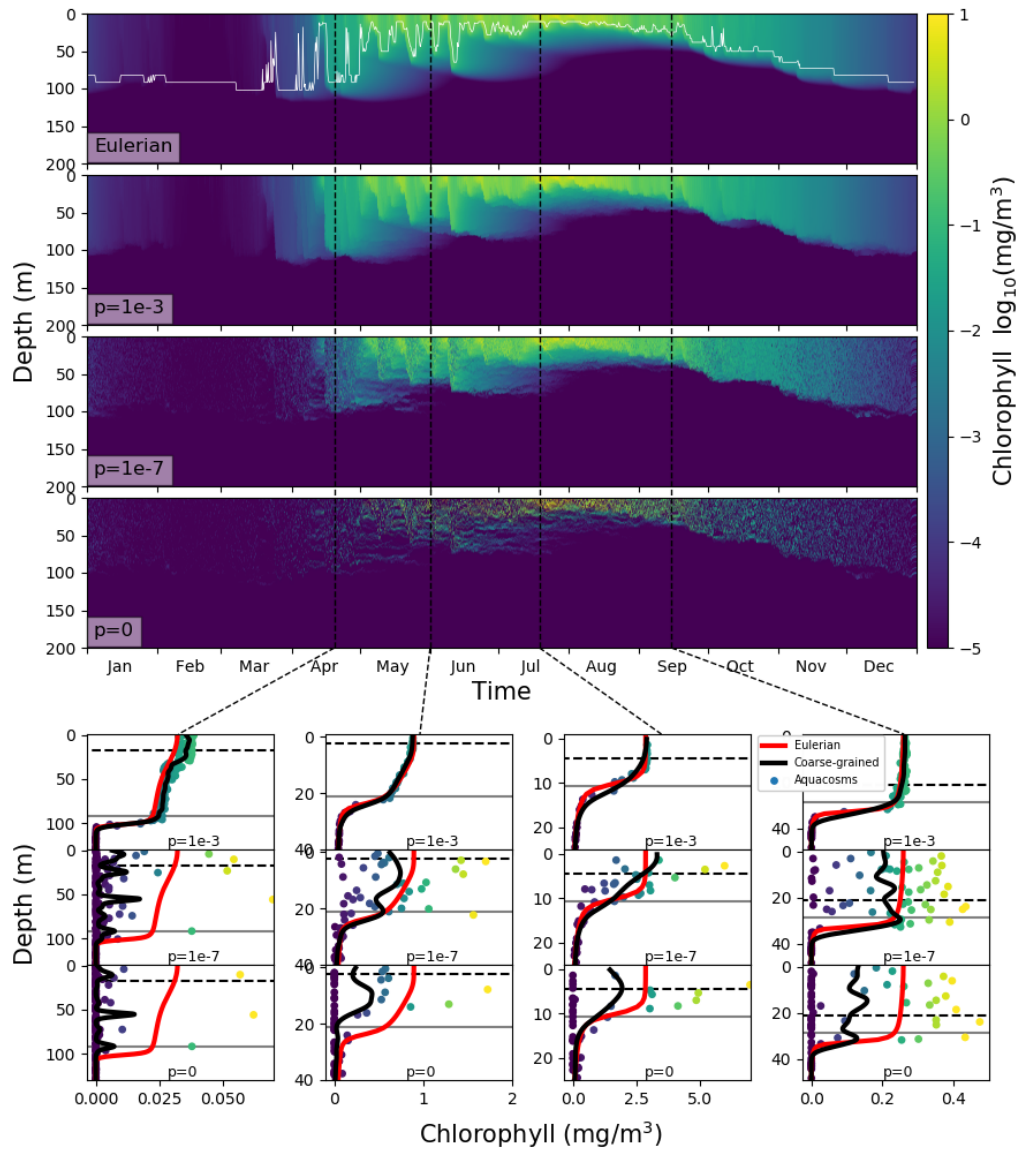


Figure S1: As Figure 6, but for the PAPA simulations.

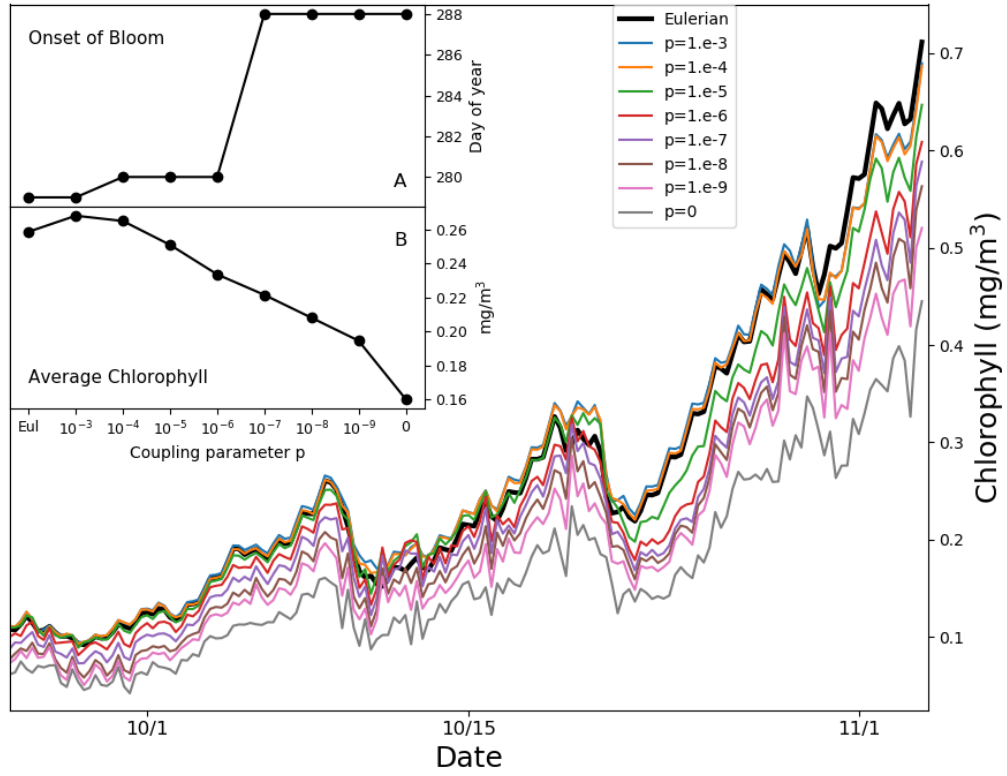


Figure S2: As figure 5, but for the SAZ simulations.

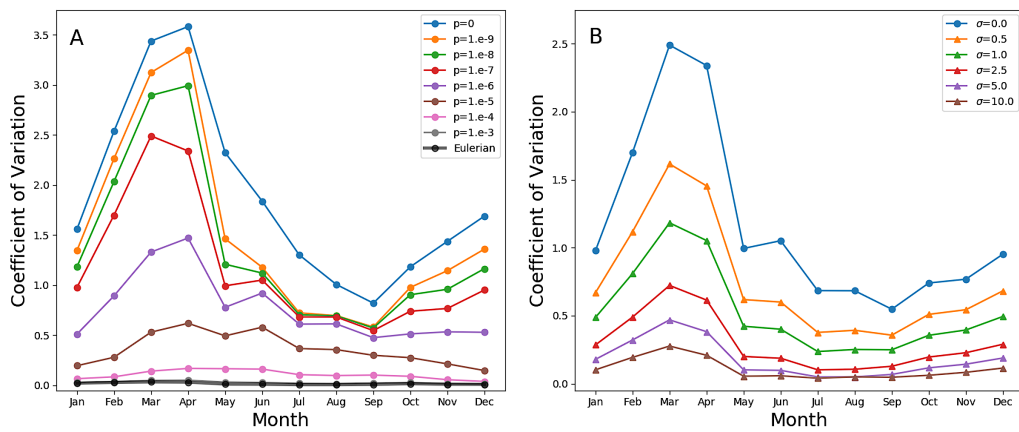


Figure S3: As Figure 7, but for the PAPA simulations.